Design of a Hyperloop System MockUp

Denis Tudor, Tony Govoni, Malicia Leipold and Mario Paolone

***Abstract*—The thorough development of the hyperloop system does require the availability of reduced-scale models. They can be used for the fast prototyping of various components, as well as for studying critical phenomena that takes place in this peculiar transportation system without the need to develop complex and expensive full-scale setups. In this respect, in this paper, we present a process for the optimal assessment of the scaling factor; it is to be used for the development of a reduced-scale hyperloop model, starting from the knowledge of the technical characteristics of its full-scale counterpart.**

The objective of the proposed process is the minimisation of the difference between the normalized power profiles associated with the reduced-scale and full-scale models of a hyperloop capsule traveling along a pre-defined trajectory with a pre-determined speed profile. By considering the hyperloop full-scale model as a reference, we propose a set of equations that link the above-mentioned metric with the constraints dictated by the kinematics of the hyperloop capsule, the capsule's battery-energy storage and propulsion systems, the capsule's aerodynamics, and the operating environmental conditions. We then derive a closed-form expression for the assessment of the optimal scaling factor and eventually use it to study the scaled-down version of an application example of a realistic hyperloop system.

I. Introduction

The use of reduced-scale (RS) model testing has been extensively adopted in several engineering disciplines to predict the behaviour of full-scale (FS) devices and structures by studying their equivalent RS models. The RS-model testing represents an efficient approach not only to reduce the cost of FS-model development but also to support fast prototyping and to study critical phenomena on the RS model before the FS model is built.

The RS-model testing relies on the similitude of physical laws, which enables the rigorous definition of the necessary conditions for designing an RS model that is equivalent to its FS counterpart. Examples of similitude laws apply to the testing of hydraulic machines [1], wind-turbine fluid dynamics [2]- [4], rocket-fluid dynamics [5]- [7], and structural engineering [8] to mention a few. With respect to the development of hyperloop systems, the use of RS models is fundamental in order to develop several components of the capsule (e.g., its propulsion system), as well as to study the influence of the operation of the infrastructure on the energy need of the whole system [9]. A first example related to the definition of a hyperloop RS model is discussed in [10]. In this paper, the authors were interested in studying the vehicle dynamics via the development of a $1/10$ scale model. By relying on the dynamic-motion similarity laws, the authors of this study investigated vertical and lateral motions of a hyperloop capsule to infer its complete dynamic characterization and to validate a corresponding numerical model.

To the best of our knowledge, the current literature has not defined suitable RS models of the whole hyperloop system in order to study the capsules' propulsion and its link with the operation of the hyperloop infrastructure. In this respect, we fill this gap by proposing a method that computes the optimal scaling factor of the physical characteristics of the capsule by taking into account the model of the hyperloop infrastructure and the model of the capsule's propulsion and kinematics [13].

As the physics laws governing the various components of a hyperloop exhibit different behaviours, with respect to a dimensional scaling process, we analyse this first fundamental aspect. The main physical phenomena that are considered are the kinematics of the hyperloop capsule, the capsule's battery-energy storage system (BESS), the propulsion system (PS), the capsule's aerodynamics, and the operating environmental conditions. We introduce and justify the metric given by the normalized aerodynamics losses, with respect to the maximum BESS power output. The link of this metric with the models of the above-mentioned physical phenomena, and with the scaling factor, results in a closed-form equation that enables the assessment of the optimal scaling factor between the FS and the RS capsules' models.

The structure of the paper is as follows: in Section II, we recall the main physical phenomena that govern the FS hyperloop model with particular references to the capsule's kinematics, BESS, PS, and aerodynamics. In Section III, we describe the RS model. In Section IV, we first introduce and justify the metric used by the scaling process; then, we illustrate the process of analytically linking the proposed metric with the FS and RS models for the optimal assessment of the scaling factor. In Section V, we illustrate an application example related to a scaling process of a realistic hyperloop system. In the last section, we conclude the paper with our final remarks and observations regarding the applicability of the proposed process.

Corresponding author's e-mail: denis.tudor@epfl.ch

Corresponding author's postal address: EPFL STI IEL DESL, ELL 117, Station 11, Route Cantonale, 1015 Lausanne, Switzerland.

Denis Tudor, Tony Govoni, Malicia Leipold and Mario Paolone are with the École Polytechnique Fédérale de Lausanne, 1015 Lausanne, Switzerland.

This paper has not been submitted elsewhere.

II. Full-Scale Hyperloop System

A. Hyperloop General Characteristics

The hyperloop is a new transportation system where vehicles travel along pre-determined trajectories and in a dedicated/confined environment (i.e., tunnels or tubes), where the pressure is kept at relatively low values (i.e., in the range of tens of mbars). These aspects are very specific to the hyperloop system hence largely differentiate it from existing modes of transportation that do not permanently isolate vehicles from the external environment. As a result, weather conditions and unexpected perturbations of an uncontrolled environment do not affect the operation of the hyperloop. Furthermore, there is the possibility of optimally controlling the pressure in a hyperloop confined environment, in conjunction with the off-line optimisation of the speed profile of the capsules. This pressure control can substantially reduce the energy needs for the operation of the whole system, thus making it the most energy-efficient transportation system for intra-continental travels [9].

Nevertheless, even if the pressure is reduced to to relatively low values, there are still some hard limitations. Indeed, the maximum speed of hyperloop capsules is limited by two main factors. The first is the ratio between the capsule's cross sections and that of the tube must be limited to ensure the flow around the capsule as it is subsonic. The second factor is the associated drag coefficient, as it limits the capsule's cruising speed for a given traction power (Indeed, such a dependency largely influences the energy required by the capsules, especially when approaching near-sonic speeds). In the following sub-sections, we first recall the limitations associated with the main aerodynamic phenomena in this system. Then, we give the fundamental equations to represent the FS hyperloop model as they are used later in the manuscript to derive the scaling process.

B. Aerodynamic Limitations of the Hyperloop System

The Hyperloop is a complex system and the definition of the RS model characteristics requires macroscopic/integral models that are subsequently translated into a specific design of the RS model.

Regarding the aerodynamics, even if a hyperloop capsule in a tube does not have an axis-symmetric geometry, the physical phenomena regarding the flow can be studied by looking at a simplified geometry allowing to study the compression of the flow around the capsule due to the reduction of the available area. Indeed, the fluid-compressibility effects play a major role in the design of high-speed hyperloop capsules as they travel in a confined environment. Indeed, as the objective is to keep the fluid around the capsule in a subsonic regime in order to limit energy consumption, the capsules' and tubes' cross sections, and/or the maximum speeds, are constrained by the compressibility of the air near the capsule. This phenomenon, called Kantrowitz Limit, is well-known [11]. In this paper, we consider capsules' speeds between $400\frac{km}{h} - 780\frac{km}{h}$ as a recent study [9] has shown detrimental effects of higher speeds on the energy used by the whole hyperloop system.

1) Problem Definition: a $2D$ slice of the 3D problem can be considered and studied as a fluid flow accelerating in a converging nozzle. The following assumptions are made:

- $2D$ steady flow;
- unidirectional flow;
- isentropic compression;
- constant heat capacity ratio of air (i.e., $\gamma_{air} = 1.4032$);
- constant specific gas constant (i.e., $r_{air} = 287[\frac{J}{kg \cdot K}]$);

The geometry of the problem is represented in Fig. 1, where $S_{fs}^{tube}[m^2]$ represents the FS cross section of the tube, $S_{fs}^{capsule}[m^2]$ represents the FS cross section of the capsule, and $A_{ext}[m^2]$ represents the difference between S_{fs}^{tube} and $S_{fs}^{capsule}$.

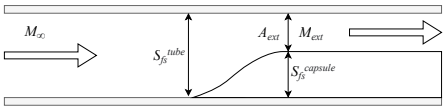

Fig. 1: Schematic $2D$ representation of a hyperloop capsule traveling in a tube.

The Mach number of the far-field flow, M_∞, can be related to (i) the speed of the capsule, $v_{fs}[\frac{m}{s}]$, and (ii) the speed of sound in the tube, $v_{sound}[\frac{m}{s}] = \sqrt{\gamma \cdot r_{air} \cdot T_\infty}$, where $T_\infty[K]$ represents the temperature of the tube's environment. Therefore, the expression of M_∞ is given here below.

$$M_\infty = \frac{v_{fs}}{\sqrt{\gamma \cdot r_{air} \cdot T_\infty}} \tag{1}$$

As the flow encounters the capsule, the cross-section available for the flow decreases. This process leads to the acceleration of the flow's speed around the capsule that, in view of the previous considerations, needs to stay subsonic.

2) Limiting Area Ratio: the main objective is to determine $A_{ext} = A_{ext}^{sonic}$. In [11] and [12], the cross section's ratio, at which the flow becomes sonic as a function of the far-field flow Mach number, is derived and recalled in (2).

$$\frac{S_{fs}^{tube}}{A_{ext}^*} = \frac{1}{M_\infty}[\frac{2}{\gamma+1}(1 + \frac{\gamma-1}{2}M_\infty)]^{\frac{\gamma+1}{2(\gamma-1)}} \tag{2}$$

Considering $S_{fs}^{tube} = S_{fs}^{capsule} + A_{ext}$ and $S_{ratio} = \frac{S_{fs}^{capsule}}{S_{fs}^{tube}}$, we need to determine S_{ratio} as a function of M_∞ for a given internal tube temperature, T_∞. The main constraint is to ensure that, for a given cross section's ratio, the flow remains subsonic everywhere around the capsule.

By referring to the Mach number limit, we need to have the airflow around the capsule cross section such as $M_{ext} = M_{lim}$. For instance, if $M_{lim} = 1$, this means we have reached the isotropic limit. Therefore, we can derive the relation that provides the dependency of S_{ratio} with M_∞ and M_{lim}, as in (3).

$$S_{ratio} = 1 - \frac{\frac{1}{M_{lim}}[\frac{2}{\gamma+1}(1+\frac{\gamma-1}{2}M_{lim})]^{\frac{\gamma+1}{2(\gamma-1)}}}{\frac{1}{M_{\infty}}[\frac{2}{\gamma+1}(1+\frac{\gamma-1}{2}M_{\infty})]^{\frac{\gamma+1}{2(\gamma-1)}}} \quad (3)$$

Fig. 2 shows the dependency of S_{ratio} with M_{∞} and M_{lim}.

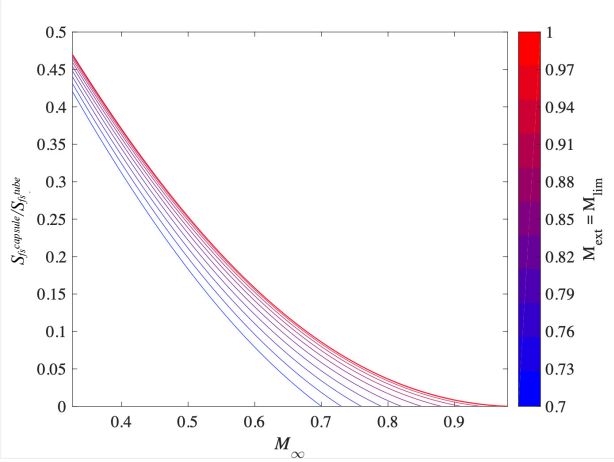

Fig. 2: Assessment of the chocked-flow regime of the fluid around the hyperloop capsule.

C. Model of the Capsule's Propulsion System

The FS tube's and capsule's models and parameters are adapted from [9]. Therefore, all the assumptions associated to the capsule's propulsion are taken from the same manuscript and not repeated here. The air-density of the full-scale infrastructure is $\rho_{fs}[\frac{kg}{m^3}]$, and the pressure inside the FS tube is $p^{fs}_{tube}[bar]$. We assume that the cross section of the tube is circular.

1) Capsule's Trajectory and Kinematic Models: as shown in Fig. 3, the length of the FS trajectory, $L_{fs}[m]$, is divided into n different zones: $\{M_1, M_2, ..., M_n\}$ each one corresponding to a given state of the capsule (i.e., acceleration, regime/constant speed, and deceleration). Along the trajectory, we can define the generic capsule's acceleration and speed, $a_{fs}[\frac{m}{s^2}]$, $v_{fs}[\frac{m}{s}]$. As done in [9], Fig. 3, shows the discrete $1D$ model of the capsule trajectory, where j and i are the space- and time-discrete sampling indexes. The trajectory's space interval $[0, L]$ is sampled at regular steps $\Delta j[m]$, $j = 0, 1, ..., \frac{L}{\Delta j}$. The corresponding time steps $\Delta i[s]$ for the capsule to travel each discrete space step are non-constant and derived from $\Delta j = v_{fs}(j-1)\Delta i + \frac{1}{2}a_{fs}(j)\Delta i^2$. As the capsule can move only forward, for each j, we can associate a corresponding unique discrete time index $i = 0, ..., t_{L_k}, ..., t_L[s]$ where $t_{L_k} = \sum_{L_k} \Delta i_k$.

2) Capsule's PS Model: In order to track a pre-defined (optimal) speed profile, we introduce the model that links the main physical characteristics of the capsule with the power necessary to propel it. The capsule is assumed to be an energy-autonomous vehicle, where the PS is formed by a BESS feeding a voltage source inverter (VSI) that is connected to a linear induction motor (LIM). The equations for modelling the behaviour of the capsule's PS can be found in [9] and [13]. Here, we introduce the main capsule's parameters, as they are functional in the scaling process:

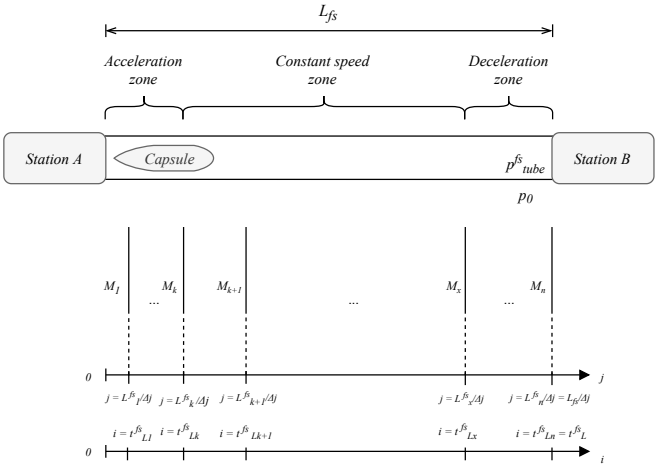

Fig. 3: Generic Trajectory of Hyperloop Capsules. Adapted from [9].

- m_0[kg]: mass of the mechanics and payload;
- N_s: number of BESS cells in series;
- N_p: number of BESS cells in parallel;
- m_{cell}[kg]: single cell mass embedding the cell's tabs wiring;
- η_{VSI}: VSI power transfer efficiency;
- η_{LIM}: LIM-to-traction power transfer efficiency;
- $P_{maxCell}$[W]: maximum power provided by a single cell;
- $k_1[\frac{kg}{W}]$: LIM weight-per-unit power density;
- $k_2[\frac{kg}{W}]$: VSI weight-per-unit power density;
- $cos(\phi)$: minimum power factor of the VSI (i.e., lowest power factor of the LIM).

The total mass of the FS capsule can be derived as a function of the aforementioned main capsule's parameters as presented in [9].

$$m_{fs} = m_0 + N_s N_p m_{cell} + \frac{1}{cos(\phi)\cdot\eta_{VSI}} P_{maxCell} N_s N_p k_2 + \\ + \frac{1}{\eta_{LIM}} P_{maxCell} N_s N_p k_1 \quad (4)$$

We can also easily define the power losses associated with the aerodynamic drag force of the FS capsule, $P^{fs}_{drag}[W]$, as in (5) (where C^{fs}_D is the drag coefficient that is a function of v_{fs}[1]). As this force is a function of the capsule's speed, it has to be defined for every discrete position, along the trajectory, of the capsule .

$$P^{fs}_{drag}(j) = \frac{1}{2} S^{capsule}_{fs} C^{fs}_D(v) \rho_{fs} v^3_{fs}(j) \quad (5)$$

[1]Note that C^{fs}_D is a function of Re for given (i.e., fixed) v_{fs} and $S^{capsule}_{fs}$.

Then, we can derive the mechanical power of the FS capsule necessary for propelling it in order to track the speed/acceleration profiles. It is worth noting that the magnetic drag has been disregarded as thrust and levitation are supposed to be both provided by the LIM as mentioned in [14]- [17].

$$P_{tr}^{fs}(j) = m_{fs}a_{fs}(j)v_{fs}(j) + P_{drag}^{fs}(j) \tag{6}$$

Finally, the electrical power that has to be provided by the BESS of the FS capsule, $P_{batt}^{fs}[W]$, can be directly related to P_{tr}^{fs} through the efficiency of the LIM, η_{LIM} and the efficiency of the VSI, η_{VSI}.

$$P_{batt}^{fs}(j) = \frac{P_{tr}^{fs}(j)}{\eta_{LIM} \cdot \eta_{VSI}} \tag{7}$$

III. Reduced-Scale Model of a Hyperloop System

This section describes how key physical phenomena of the hyperloop system are scaled-down. We refer, in particular, to the capsule's (i) masses, (ii) kinematic model, (iii) power profiles, (iv) BESS energy capacity, and (v) aerodynamics.

More specifically, we first introduce the definition of the scaling factor. Then, we discuss the scaling of the capsule's kinematic model, its masses, power profiles, and environment operating conditions. We separately discuss the scaling of the capsule's aerodynamics, as it requires a dedicated section, in view of the need for numerical assessing its dependency with the scaling factor and the capsule's speed.

A. Scaling of the Capsule's Kinematic Model, Masses, Power Profiles, and Environment

Let $k \in \mathbb{R}^+$ the scale factor, with $k > 1$. Distances, speeds, accelerations, time and masses of the RS model, as well as environmental conditions, power profiles, and BESS energy capacity, can be derived in a straightforward way.

1) Distances, Speeds, Accelerations, Time, and Masses: As the times of the RS and FS models are unaltered by the scaling process, the kinematic quantities of the capsule's RS model can be directly linked to the corresponding ones of the FS model, as in (8).

$$\begin{cases} t_L^{rs} = t_L^{fs} \\ v_{rs} = \frac{v_{fs}}{k} \\ a_{rs} = \frac{a_{rs}}{k} \\ L_{rs} = \frac{L_{fs}}{k} \end{cases} \tag{8}$$

Regarding the masses of the RS model, as in [10], [18]- [20], we assume that the components of the capsule have to maintain the same relative density factor of their materials. As the RS and FS models are characterised by materials with the same volumetric densities, the overall mass of the capsule RS model, $m_{rs}[kg]$, is inversely proportional to the cube of the scaling factor times the mass of the capsule FS model, m_{fs} (see (9)). In other words, the overall mass of the RS capsule model scales-down like its overall volume does.

$$m_{rs} = \frac{m_{fs}}{k^3} \tag{9}$$

2) Tube Environment: the operational conditions of the RS tube, namely the air-density $\rho_{rs}[\frac{kg}{m^3}]$ and temperature, are assumed to be identical to those of the FS. The same consideration applies to the tube's pressure, $p_{tube}^{rs}[bar]$. The RS cross section of the tube varies with the FS cross section of the tube, as shown in (10).

$$\begin{cases} \rho_{rs} = \rho_{fs} \\ p_{tube}^{rs} = p_{tube}^{fs} \\ S_{tube}^{rs} = \frac{S_{tube}^{fs}}{k^2} \end{cases} \tag{10}$$

3) Powers: The power losses due to the aerodynamic drag force in the RS model can be defined similarly to (5), for every discrete position of the capsule along the RS trajectory and, as a function of the RS model, the drag coefficient C_D^{rs} and speed $v_{rs}[\frac{m}{s}]$. Note that, in (11), the drag coefficient cannot be directly linked to the RS capsule speed in a closed form. This aspect is discussed in the following sub-section.

$$\begin{aligned} P_{drag}^{rs}(j) &= \frac{1}{2}S_{rs}^{capsule}C_D^{rs}(v)\rho_{rs}v_{rs}^3(j) = \\ &= \frac{1}{2}\frac{S_{fs}^{capsule}}{k^2}C_D^{rs}(v_{rs})\rho_{fs}\frac{v_{fs}^3(j)}{k^3} \end{aligned} \tag{11}$$

The mechanical power of the capsule is defined in (12).

$$\begin{aligned} P_{tr}^{rs}(j) &= m_{rs}a_{rs}(j)v_{rs}(j) + P_{drag}^{rs}(j) = \\ &= \frac{m_{fs}}{k^3}\frac{a_{fs}(j)v_{fs}(j)}{k^2} + P_{drag}^{rs}(j) \end{aligned} \tag{12}$$

The electrical power provided by the BESS RS model, $P_{batt}^{rs}[W]$, is directly related to P_{tr}^{rs} through the VSI power-transfer efficiency, η_{VSI}, and the LIM-to-traction power-transfer efficiency, η_{LIM}. As we will see later, the values of these two efficiencies in the RS and FS models do not play any role.

$$P_{batt}^{rs}(j) = \frac{P_{tr}^{rs}(j)}{\eta_{LIM} \cdot \eta_{VSI}} \tag{13}$$

B. Scaling of the Capsule's Aerodynamics and Drag Coefficient

The drag coefficient of the RS capsule, C_D^{rs}, is a coefficient that takes into account the flow behaviour around a specific object. C_D^{rs} models the effects of the pressure and viscous forces parallel to the flow direction exerted on the capsule's surface. Although it can be defined as in (14), as a function of the previously introduced quantities and parameters of both RS and FS models, the drag force $F_{drag}^{rs}(k, \frac{v_{fs}}{k})[N]$ does not have a closed-form expression that links it to the scaling factor k (e.g., [5]- [7]). Such a link has to be quantified numerically by means of a dedicated computational fluid dynamics (CFD) analysis, as a function of the scaling factor k or, in case, that is determined experimentally.

$$C_D^{rs} = \frac{2 \cdot F_{drag}^{rs}(k, v_{rs})}{\rho_{rs}v_{rs}^2 S_{rs}^{capsule}} = \frac{2 \cdot F_{drag}^{rs}(k, \frac{v_{fs}}{k})}{\rho_{fs}\frac{v_{fs}^2}{k^2}\frac{S_{fs}^{capsule}}{k^2}} \tag{14}$$

More specifically, we have carried-out a CFD analysis by using the COMSOL© Multiphysics simulation environment, with respect to a discrete set of values of the scaling factor k that starts from a given shape of the FS capsule's aeroshell and tube diameter. The single-phase turbulent flow was solved using a Reynolds-averaged Navier-Stokes (RANS) Low Reynolds k-ϵ model, because large Eddy simulations (LES) were too computationally demanding. We have selected this model because it provides a good compromise between computation time, resources, robustness, and accuracy of results. It is worth saying that a comparison between the two models is beyond the scope of this manuscript.

The simulations refer to a steady-state condition at the capsule's cruising speed. Such a condition was selected as the capsule spends the majority of the time in this state.

Section V contains all the results regarding this specific set of simulations as it enables us to make a numerical quantification of the function $C_D^{rs}(k)$.

IV. Optimal Assessment of the Scaling Factor

In order to optimally determine the scaling factor k, there is the need to determine a specific metric to be minimised. To define such a metric, there are two fundamental considerations to take into account: (i) the hyperloop system should achieve the least possible energy use per passenger-per-km, and (ii) the high speed achieved by the capsule requires substantial power provided by the on-board BESS. Therefore, the FS and RS capsule models should be characterised by the same energy that is normalised by the maximum power output of the BESS (as this device is the only power source of the capsules). In other words, if we define $E_{norm}^{fs} = \int \frac{P_{batt}^{fs}(t)}{max(P_{batt}^{fs}(t))}\,dt$ as the normalized energy consumption of the FS capsule and $E_{norm}^{rs} = \int \frac{P_{batt}^{rs}(t)}{max(P_{batt}^{rs}(t))}\,dt$ as the normalized energy consumption of a RS capsule, these two values have to be as similar as possible.

As the time for the RS and FS models are unaltered by the scaling process, we can transform the above-mentioned metric in terms of powers provided by the FS and RS capsules' BESSs. In other words, we seek the least difference between the normalised power profiles of the RS and FS models.

This similarity cannot be guaranteed all along the trajectory (essentially due to the non-linear relations of the power profiles with the scaling factor and capsules' speeds). Therefore, we will require it with respect to the capsule's cruising speed as in (15).

$$\begin{aligned} \min_{k} \quad & (f(k) = \frac{P_{batt}^{rs}(k, v_{max}^{rs})}{max(P_{batt}^{rs}(k))} - \frac{P_{batt}^{fs}(v_{max}^{fs})}{max(P_{batt}^{fs})}) \\ \text{subject to} \quad & (5)-(7), (10)-(13) \end{aligned} \tag{15}$$

In view of (11), (12), and (13), and by recalling that at cruising speed the capsule acceleration is null, the first term of the objective function, say T_1 in (15), can be written as in (16).

$$\begin{aligned} T_1 &= \frac{P_{batt}^{rs}(k, v_{max}^{rs})}{max(P_{batt}^{rs}(k))} \\ &= \frac{\frac{P_{tr}^{rs}(k, v_{max}^{rs})}{\eta_{LIM}\cdot\eta_{VSI}}}{\frac{P_{tr,max}^{rs}}{\eta_{LIM}\cdot\eta_{VSI}}} \\ &= \frac{P_{tr}^{rs}(k, v_{max}^{rs})}{P_{tr,max}^{rs}} \\ &= \frac{S_{fs}^{capsule} C_D^{rs}(k; \frac{v_{max}^{fs}}{k}) \rho_{fs} (v_{max}^{fs})^3}{max(2m_{fs} a_{fs}(\hat{j}) v_{fs}(\hat{j}) + S_{fs}^{capsule} C_D^{rs}(k; v_{rs}(\hat{j})) \rho_{fs} v_{fs}^3(\hat{j}))} \end{aligned} \tag{16}$$

where the index $\hat{j}$ refers to the position that, along the trajectory, corresponds to the maximum value of the P_{batt}^{rs}.

In view of (5), (6), and (7), and by recalling that at cruising speed the capsule acceleration is null, the second term of the objective function, say T_2 in (15), can be written as in (17).

$$\begin{aligned} T_2 &= \frac{P_{batt}^{fs}(v_{max}^{fs})}{max(P_{batt}^{fs})} \\ &= \frac{\frac{P_{tr}^{fs}(v_{max}^{fs})}{\eta_{LIM}\cdot\eta_{VSI}}}{\frac{P_{tr,max}^{fs}}{\eta_{LIM}\cdot\eta_{VSI}}} \\ &= \frac{P_{tr}^{fs}(v_{max}^{fs})}{P_{tr,max}^{fs}} \\ &= \frac{S_{fs}^{capsule} C_D^{fs}(v_{max}^{fs}) \rho_{fs} (v_{max}^{fs})^3}{max(2m_{fs} a_{fs}(\hat{j}) v_{fs}(\hat{j}) + S_{fs}^{capsule} C_D^{fs}(v_{fs}(\hat{j})) \rho_{fs} v_{fs}^3(\hat{j}))} \end{aligned} \tag{17}$$

Note that, in view of the above, the objective function presented in (15) is independent of both the VSI power-transfer efficiency η_{VSI} and the LIM-to-traction power-transfer efficiency η_{LIM}, even if these two efficiencies are different in the FS and RS models. Therefore, η_{LIM} and η_{VSI} do not play any role in the scaling-down process.

Here, we apply (15) to determine the optimal scaling factor for a realistic hyperloop test case.

V. Application Example

A. Full-Scale Model Assumptions

1) Main Numerical Assumptions: in order to apply the proposed process for infering the scaling factor, we refer to an FS hyperloop system whose characteristics have been determined in [9]. More specifically, (18) provides a summary of the main parameter of such a system. Furthermore, Fig. 4 shows the FS acceleration profile, $a_{fs}(i)$, where the maximum acceleration is slightly below $1.5\frac{m}{s^2}$. Fig. 5 shows the FS model speed profile $v_{fs}(i)$ where the maximum (cruising) speed is equal to $600\frac{km}{h}$. In Fig. 6, the FS model power-time profile of the traction and BESS, respectively, $P_{tr}^{fs}(i)$ and $P_{batt}^{fs}(i)$, are also presented. The maximum value of $P_{batt}^{fs}(i)$ along the trajectory is $6MW$. Note that the parameter C_D^{fs} was validated within the CFD simulation, at the given v_{mas}^{fs} speed.

$$\begin{cases} \eta_{LIM} = 0.65 \\ \eta_{VSI} = 0.95 \\ L_{fs} = 500km \\ S_{fs}^{capsule} = 3.14m^2 \\ S_{fs}^{tube} = 12.56m^2 \\ p_{tube}^{fs} = 50.53mbar \\ m_{fs} = 21243.47kg \\ t_L^{fs} = 53.75minutes \\ v_{max}^{fs} = 594.4\frac{km}{h} \\ C_D^{fs} = 0.51 \end{cases} \quad (18)$$

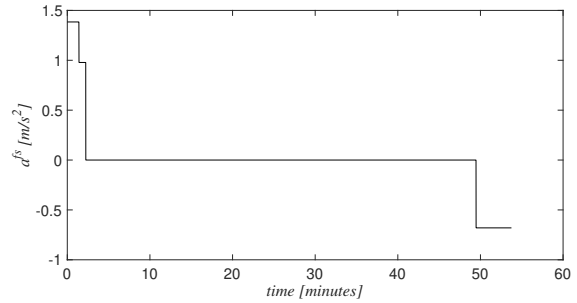

Fig. 4: FS hyperloop model acceleration profile as a function of time, $a_{fs}(i)$. Adapted from [9] for a hyperloop trajectory length $L_{fs} = 500km$.

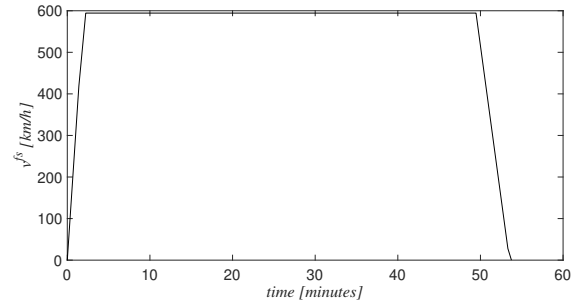

Fig. 5: FS hyperloop model speed profile as a function of time, $v_{fs}(i)$. Adapted from [9] for a hyperloop trajectory length $L_{fs} = 500km$.

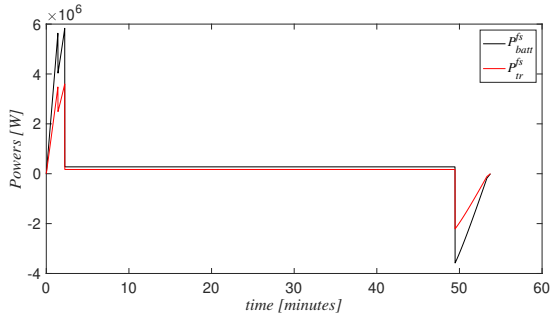

Fig. 6: FS hyperloop model traction and BESS power profiles as functions of time, $P_{tr}^{fs}(i)$ and $P_{batt}^{fs}(i)$.

$k[-]$	$C_D^{rs}[-]$
4	0.4327
5	0.4189
6	0.4188
7	0.4139
9	0.4343
11	0.4668
12	0.5679
14	0.7834
16	0.9156
18	1.0397

TABLE I: CFD-determined values of $C_D^{rs}(k, \frac{v_{max}^{fs}}{k})$.

B. Reduced-Scale Model Assumptions

1) Aerodynamics: A hyperloop capsule aeroshell was specifically designed. Its shape is shown in Fig. 7.

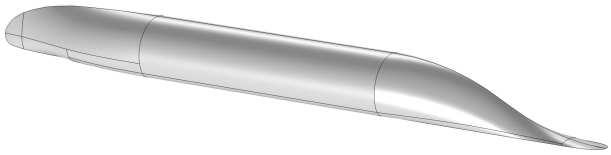

Fig. 7: Aeroshell model

Specific CFD simulations were carried out with the following assumptions: (i) the simulation domain is composed of a half tube from which the capsule was subtracted (we take advantage of the model symmetry), and (ii) the simulation domain comprises air at $T_0 = 293.15K$ and $p_{tube}^{rs} = 50.53mbar$.

CFD simulations were carried out for various values of k to numerically infer the dependency $C_D^{rs}(k, \frac{v_{max}^{fs}}{k})$, where the imposed velocity of the air at the inlet of the simulation domain was adapted for each k as in (8). The value of the FS capsule cruising speed, v_{max}^{fs}, is the one reported in (18). The values of $C_D^{rs}(k, \frac{v_{max}^{fs}}{k})$ for $k = \{4, 5, 6, 7, 9, 11, 12, 14, 16, 18\}$ are given in Table I. These discrete values of $C_D^{rs}(k, \frac{v_{max}^{fs}}{k})$ were linearly interpolated as shown in Fig. 8. The sudden increase in drag coefficient, as a function of k for values larger than $k = 11$, can be interpreted as the transition to a laminar-flow field around the RS model. The skin-friction drag becomes predominant no matter the shape of the aeroshell, as it is an intrinsic limitation of the scaling process.

C. Results

The values of the objective function of the problem (15) are shown in Fig. 9. It is interesting to note that any RS model with $4 \leq k \leq 11$ can produce satisfactory results with respect to the minimisation of the metric proposed in the paper. Therefore, RS hyperloop models with a relatively broad range of scaling factors can be considered.

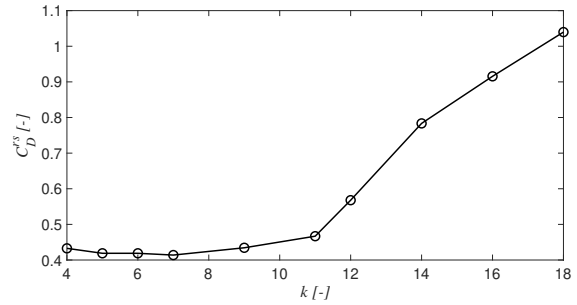

Fig. 8: Interpolated values of $C_D^{rs}(k, \frac{v_{max}^{fs}}{k})$ for various values of the scaling factor, k.

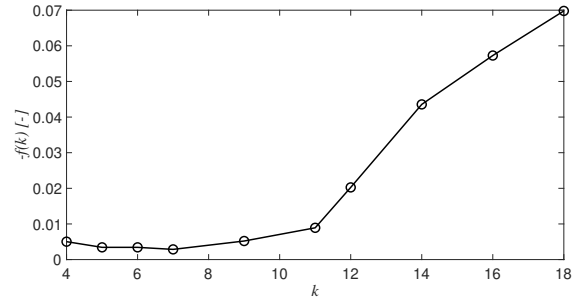

Fig. 9: Values of the objective function of the problem (15) for various values of the scaling factor, k.

The normalized-power profiles, as functions of time, are shown in Fig. 10 for different values of the scaling factor (the FS normalised power profile, i.e., for $k = 1$, is reported as well). In the constant-speed zone, the proximity of the normalised powers for $4 \leq k \leq 11$ with the FS one can be clearly seen. Fig. 11, shows the speed profiles (always as a function of time) for the same values of the scaling factor, whereas Fig. 12 and Fig. 13 show the acceleration and the non-normalised power profiles, respectively.

It is interesting to note that, for the selected values of the scaling factor, the RS model's maximum speeds vary between $33 - 149\frac{km}{h}$, whereas the RS model's masses vary between $3 - 332kg$, as shown in TABLE II. The maximum power provided by the RS BESS models varies between $3.4 - 5702W$. These values of speeds and BESS powers are certainly easy to handle by a dedicated RS hyperloop mockup.

VI. Conclusions

The development of an FS hyperloop prototype system is an expensive and time-consuming process that entails limited flexibility of the realised setup. In this respect, we have proposed a suitable framework that is capable of determining not only the scaling factor but also the main variables and parameters of a hyperloop mockup. More specifically, the proposed framework relies on the operating conditions of the hyperloop infrastructure and the models of the capsule's kinematics, BESS, PS and aerodynamics.

$k[-]$	$m_{rs}[kg]$
4	331.92
5	169.94
6	98.34
7	61.93
9	29.14
11	15.96
12	12.29
14	7.74
16	5.18
18	3.64

TABLE II: RS mass values, m_{rs} function of k.

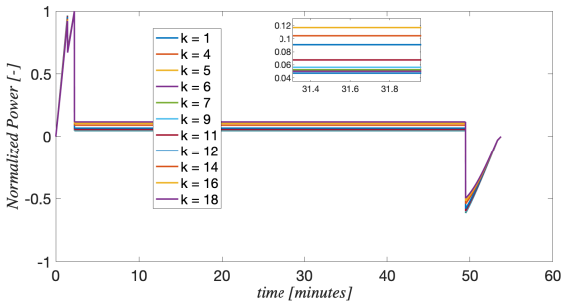

Fig. 10: Normalized power profiles as functions of time of both FS and RS hyperloop models for the considered values of the scaling factor k.

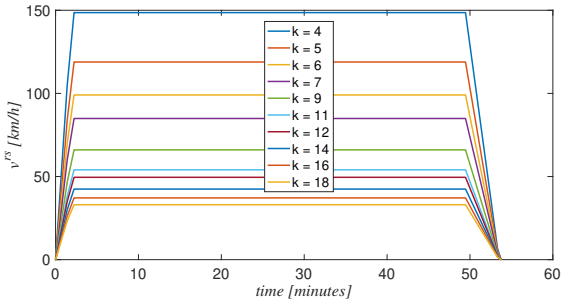

Fig. 11: Speed profiles as functions of time of the hyperloop RS model for the various considered values of the scaling factor k.

By introducing a suitable metric that takes into account both the energy and power demands of the hyperloop FS and RS capsules, we have shown how the above operating conditions and models can be used to optimally determine the scaling factor of the hyperloop RS model. Furthermore, we have discussed and assessed the importance of the hyperloop capsule's aerodynamics, with respect to the scaling process, and the means of integrating a numerical CFD analysis into the proposed framework.

By making reference to an FS hyperloop system whose characteristics were already determined in a previous study (i.e., capsule's maximum speeds of $600km/h$, capsule's mass

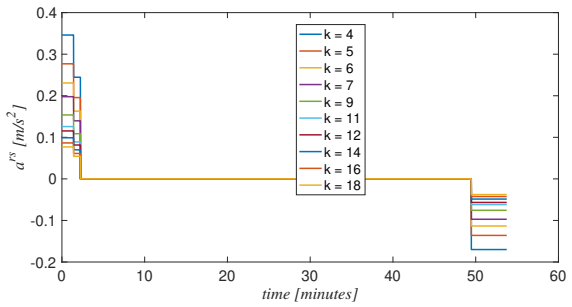

Fig. 12: Acceleration profiles as functions of time of the hyperloop RS model for the various considered values of the scaling factor k.

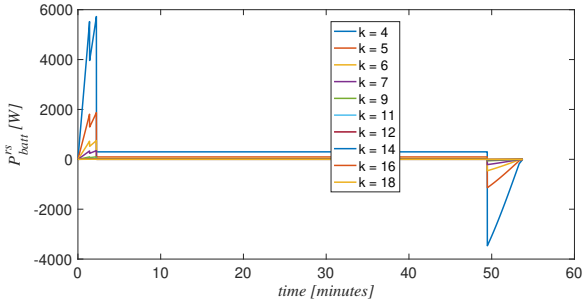

Fig. 13: Power profiles as functions of time of the hyperloop RS model for the various considered values of the scaling factor k.

of $22tons$ and maximum BESS power of $6MW$), in the proposed framework, we have identified a range of values of the scaling factor, i.e., $4 \leq k \leq 11$; it is quite large. Within such an interval, the objective function of the proposed framework does not exhibit substantial changes and gives an opportunity to the modeler to adopt the value of the scaling factor that is more convenient, as the maximum BESS power of the RS model vary between $3.4 - 5702W$ with speeds between $33 - 149km/h$.

Future work will be focused on the construction of an RS hyperloop mockup by using the proposed framework. Such an RS hyperloop model will be used to study the viability of the various technical solutions of the FS hyperloop system in an efficient way, as it simplifies the fast prototyping of various components of the hyperloop capsules and infrastructure.

REFERENCES

[1] International Electrotechnical Commission IEC (2019) "International Standard IEC 60193: Hydraulic turbines, storage pumps and pump-turbines - model acceptance tests", Edition 3.0, 2019-04.

[2] W. Yossri, S. Ben Ayed and A. Abdelkefi, "Three-dimensional computational fluid dynamics investigation on size effect of small-scale wind turbine blades", AIAA Scitech 2021 Forum, 11–15 and 19–21 January 2021.

[3] T. Revaz, M. Lin and F. Porté-Agel, "Numerical Framework for Aerodynamic Characterization of Wind Turbine Airfoils: Application to Miniature Wind Turbine WiRE-01", Energies 2020, 13, 5612.

[4] M. Bastankhah and F. Porté-Agel, "A New Miniature Wind Turbine for Wind Tunnel Experiments. Part I: Design and Performance", Energies 2017, 10, 908.

[5] M.-C. Gauffre, H. Neau, O. Simonin, R. Ansart, N. Meyers and S. Petitot, "Numerical Simulation of Dome Filling in an Experimental Rocket Engine Mockup", Journal of Propulsion and Power, Vol. 30, No. 3, May–June 2014.

[6] V. Zubanov, V. Egorychev, L Shabliy, "Design of Rocket Engine for Spacecraft Using CFD-Modeling", Procedia Engineering, Volume 104, 2015, Pages 29-35.

[7] H. Nagata, T. Uematsu, K. Ito, "CAMUI Type Hybrid Rocket as Small Scale Ballistic Flight Testbed", Transactions of the Japan Society for Aeronautical and Space Sciences, Aerospace Technology Japan, 2012, Volume 10, March 2012.

[8] A. Casaburo, G. Petrone, F. Franco, and S. De Rosa, "A Review of Similitude Methods for Structural Engineering", ASME. Appl. Mech. Rev. May 2019; 71(3): 030802.

[9] Denis Tudor, Mario Paolone, "Operational-Driven Optimal-Design of a Hyperloop System", Transportation Engineering, 2021, 100079, ISSN 2666-691X.

[10] Lee, J.; You, W.; Lim, J.; Lee, K.-S.; Lim, J.-Y. "Development of the Reduced-Scale Vehicle Model for the Dynamic Characteristic Analysis of the Hyperloop", Energies 2021, 14, 3883.

[11] J. Oh, T. Kang, S. Ham, K. S. Lee, Y. J. Jang, H. S. Ryou and J. Ryu, "Numerical Analysis of Aerodynamic Characteristics of Hyperloop System," in Energies 12(3):518, February 2019.

[12] Yang Sui, Jiqiang Niu, Qiujun Yu, Yanping Yuan, Xiaoling Cao, Xiaofeng Yang, "Numerical analysis of the aerothermodynamic behavior of a Hyperloop in choked flow", Energy, Volume 237, 2021, 121427, ISSN 0360-5442.

[13] D. Tudor and M. Paolone, "Optimal Design of the Propulsion System of a Hyperloop Capsule", in IEEE Transactions on Transportation Electrification, vol. 5, no. 4, pp. 1406-1418, Dec. 2019.

[14] T. Morizane, K. Tsujikawa, and N. Kimura, "Control of Traction and Levitation of Linear Induction Motor Driven by Power Source With Frequency Component Synchronous With the Motor Speed," IEEE Transactions on Magnetics, vol. 47, no. 10, pp. 4302–4305, Oct. 2011, Conference Name: IEEE Transactions on Magnetics.

[15] S. Nakatani, D. Okamori, T. Morizane, and H. Omori, "Dynamic Characteristics Verification of Linear Induction Motor by Simultaneous Propulsion and Levitation Control," in 2020 22nd European Conference on Power Electronics and Applications (EPE'20 ECCE Europe), Sep. 2020, P.1–P.10.

[16] S. Nakatani, K. Sannomiya, D. Okamori, T. Morizane, N. Kimura, and H. Omori, "Experimental Confirmation of Speed and Air Gap Control with Only Linear Induction Motor for Levitation," in 2019 12th International Symposium on Linear Drives for Industry Applications (LDIA), Jul. 2019, pp. 1–5.

[17] S. Nakatani, D. Okamori, and T. Morizane, "Verification of Control Performance when Driving Linear Induction Motor with Superimposed Frequency," in 2020 International Conference on Electrical Machines (ICEM), ISSN: 2381-4802, vol. 1, Aug. 2020, pp. 1246–1250.

[18] Joseph R. Chambers, "The Role of Dynamically Scaled Free-Flight Models in Support of NASA's Aerospace Programs," NASA SP 2009-575.

[19] Gang Wang, Minghui Zhang, Yujin Tao, Jie Li, Dong Li, Yizhe Zhang, Changsheng Yuan, Weimin Sang, Binqian Zhang, "Research on analytical scaling method and scale effects for subscale flight test of blended wing body civil aircraft," Aerospace Science and Technology, Volume 106, 2020, 106114, ISSN 1270-9638.

[20] Gary Weaks, "Weight and flight performance of scale models," Technical Report [online], https://bit.ly/37akCyi.

[21] J. Oh, T. Kang, S. Ham, K. S. Lee, Y. J. Jang, H. S. Ryou and J. Ryu, "Numerical Analysis of Aerodynamic Characteristics of Hyperloop System," in Energies 12(3):518, February 2019.

[22] Neural Concepts, "Deep Learning for Enhanced Engineering," Technical Report [online], https://www.neuralconcept.com/.